NEUTRON STAR PRECESSION

Ira Wasserman, Cornell University

Collaborating with:

J. Cordes

T. Akgun

A. Sedrakian

B. Link (in progress)

R. Epstein

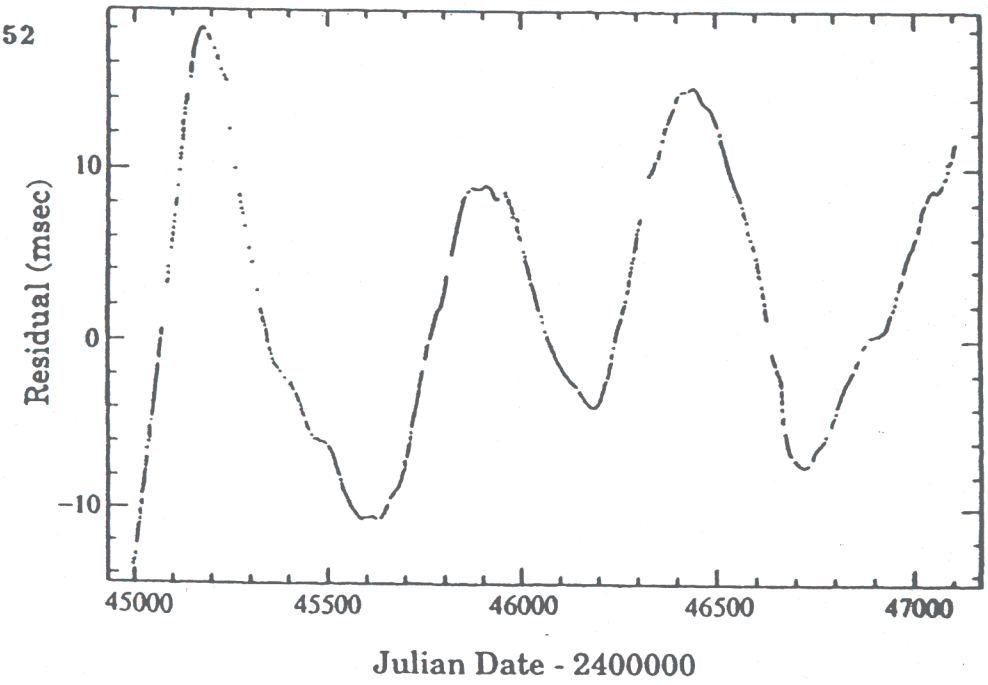

Crab
Lyne
et al.

FIGURE V Phase residuals from the Crab pulsar (after Lyne, Pritchard, and Smith 1988).

Vela X-mas '88

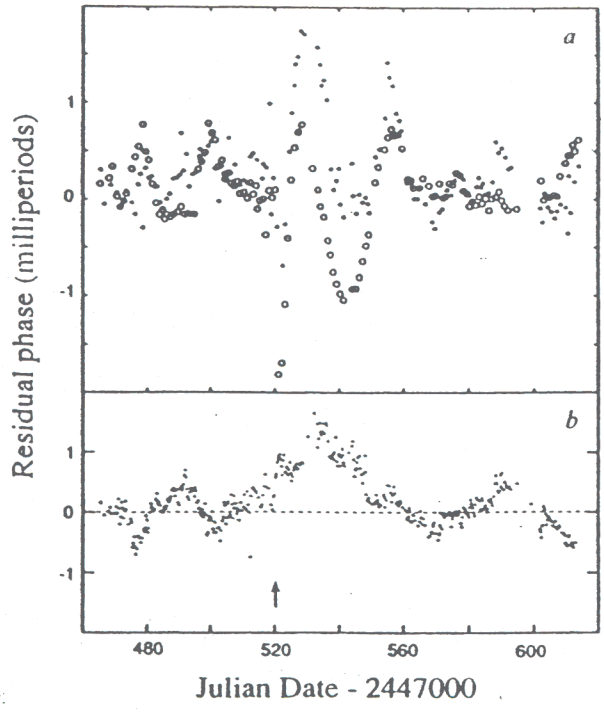

FIG. 2 *a*, The residuals from the fit using equation (3); O, 950 MHz; ●, 635 MHz. Each point is the average of one day's data: *b*, The phase difference obtained by subtracting the 950-MHz arrival times from the 635-MHz arrival times (positive value indicates that 635-MHz data arrived later). The arrow shows the epoch of the glitch.

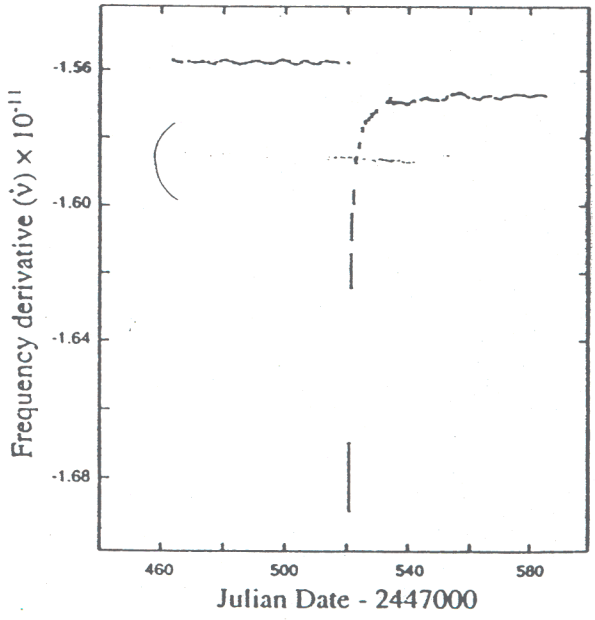

FIG. 3 The variation of frequency derivative $\dot{\nu}$ with time. The error bars are $\pm 2\sigma$. Values were obtained by fitting for ν and $\dot{\nu}$ to sequences of 8 days of data, and advancing by one day between each fit. The values of $\dot{\nu}$ immediately before and after the jump were calculated using the parameters given in Table 1.

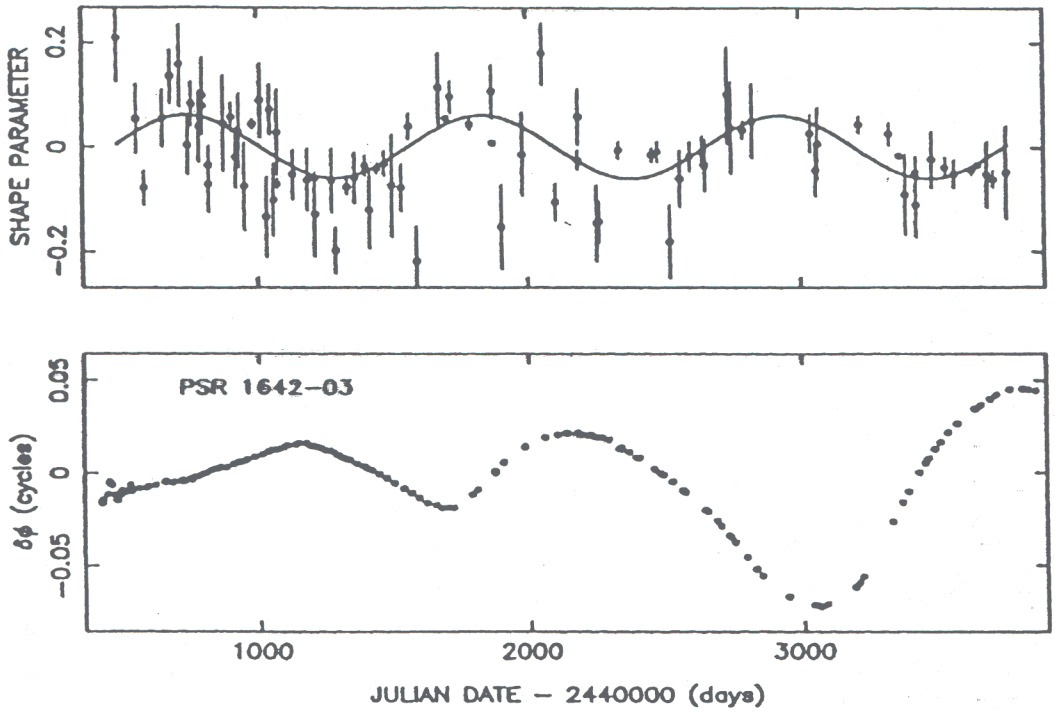

1642-03
Blaskiewic
& Cordes

FIGURE VI Evidence for free precession from PSR1642−3. (Bottom) Phase residuals after second order fit; (Top) Pulse shape parameter vs. time. The solid curve is the best fit sinusoid implied by Fourier analysis of the time series.

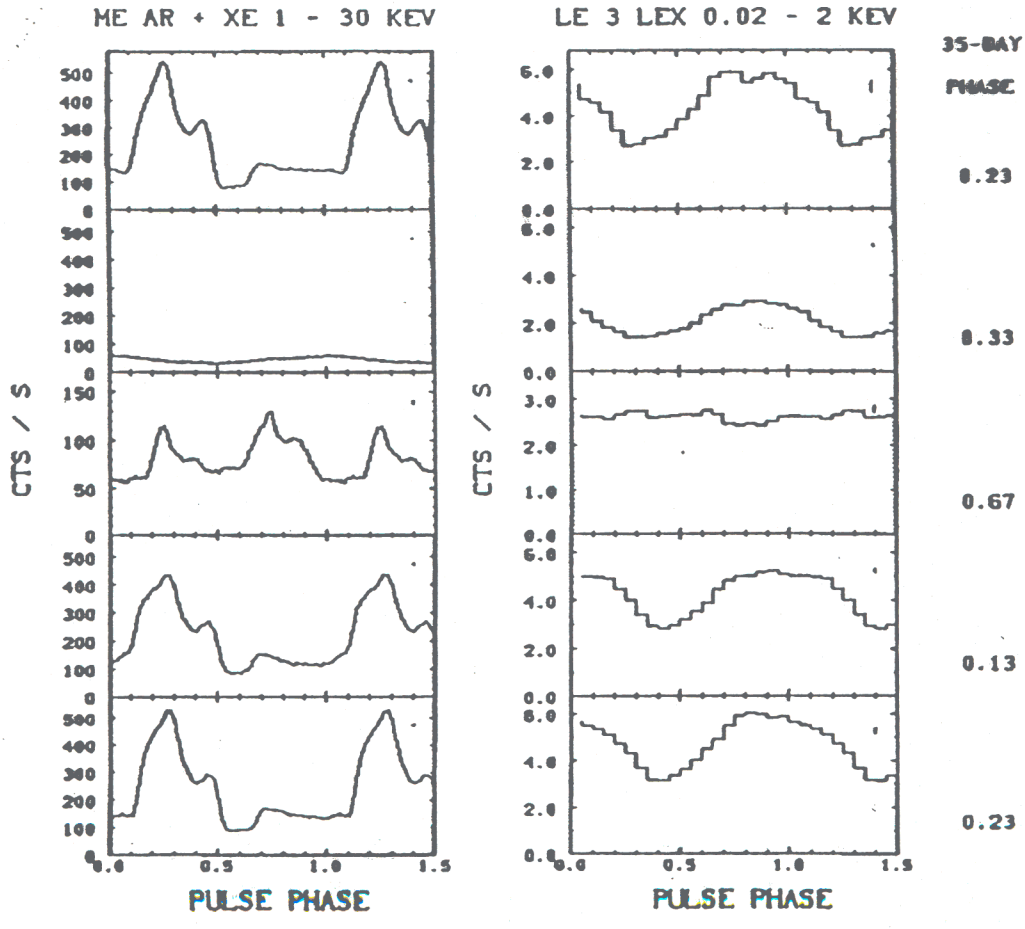

Her X-1
Trümper et al.

FIG. 1.—Light curves of the L24 a pulses observed at various phases of the 35 day cycle for (*a*) hard X-rays (ME) in the range 1–30 keV; (*b*) soft X-rays (LE with 3000 Å Lexan filter) in the range 0.02–2 keV. The scale of the ME and LE light curves at $\Psi_{35} = 0.67$ (short-on state) has been magnified by a factor of 4 and 2, respectively. The typical statistical errors are indicated at the upper right-hand corner of each curve. The 35 day phase Ψ_{35} (measured with respect to turn-on), which progresses from top to bottom, is also indicated for each pair of ME, LE pulse shapes.

1642-03
30 yrs
Shabanova,
Lyne &
Urama
(2001)

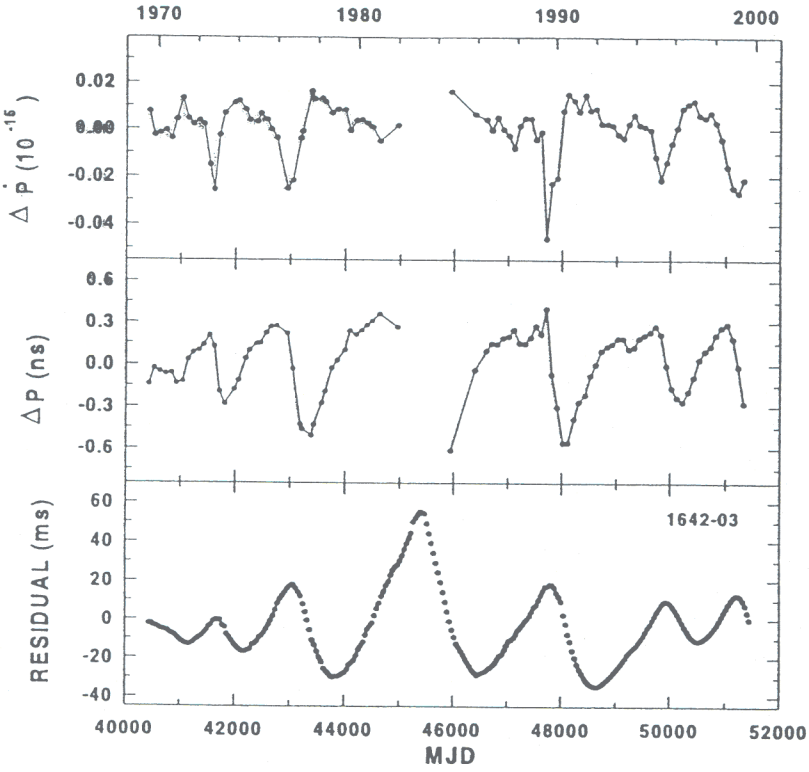

FIG. 3.—Period derivative residuals, $\Delta\dot{P}$, period residuals, ΔP, and timing residuals over 30 years of observations relative to the spin-down model given in Table 1.

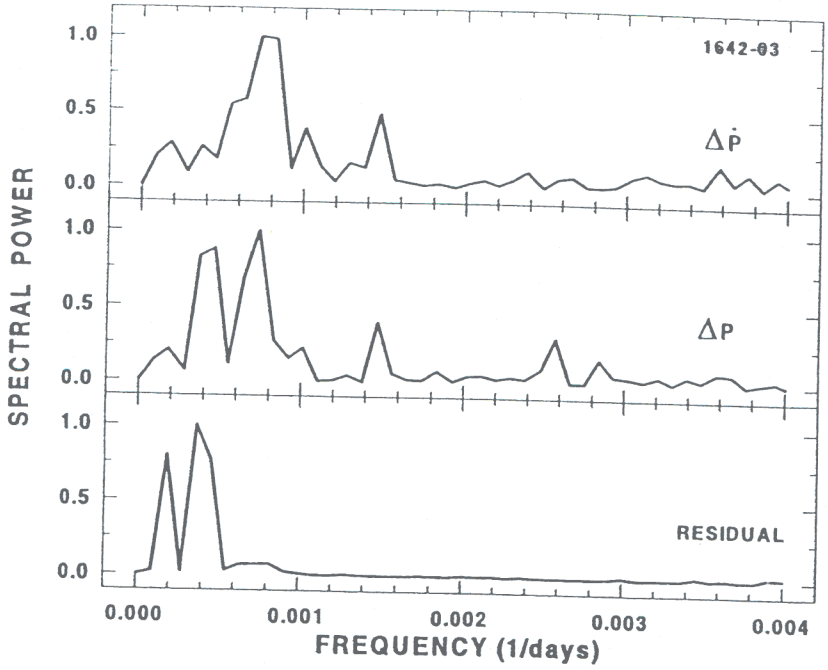

FIG. 4.—Power spectrum of the period derivative residuals, the period residuals, and the timing residuals obtained by using the Fourier transforms technique. Spectral power of the residuals has arbitrary normalization. The spectra exhibit wide spectral features at multiple frequencies of approximately 0.0004 and 0.0008 day^{-1}, corresponding to 2500 and 1250 days, respectively.

1828-11

Stairs et al. 2000

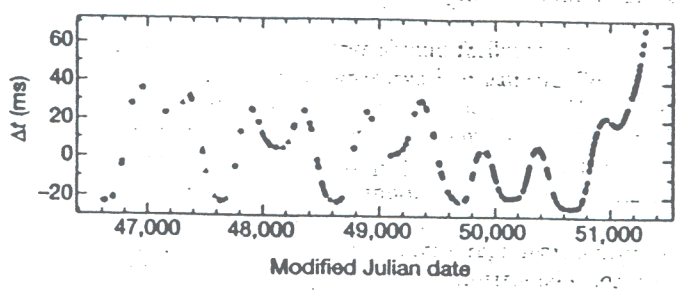

Figure 1 Post-fit timing residuals Δt for PSR B1828–11 after fitting for the spin-down parameters given in Table 1. Each point represents an observation of roughly 30 minutes' duration at a frequency around 1,400 MHz (circles) or 1,600 MHz (triangles). Individual profiles are described by a linear combination of two extreme standard profiles, one wide, one narrow. An iterative frequency-domain routine was used to determine the relative strengths of the standard profiles required to synthesize the daily profiles. This provides a 'shape parameter', $S = \frac{A_N}{A_N + A_W}$, where A_N and A_W are the fitted heights of the narrower and wider standard profiles respectively, so that $S \sim 1$ for the narrowest pulses and $S \sim 0$ for wider ones. The pulse times-of-arrival (TOAs) are also derived from this shape-fitting procedure; the errors in the TOAs are limited by random noise to about 0.2 ms.

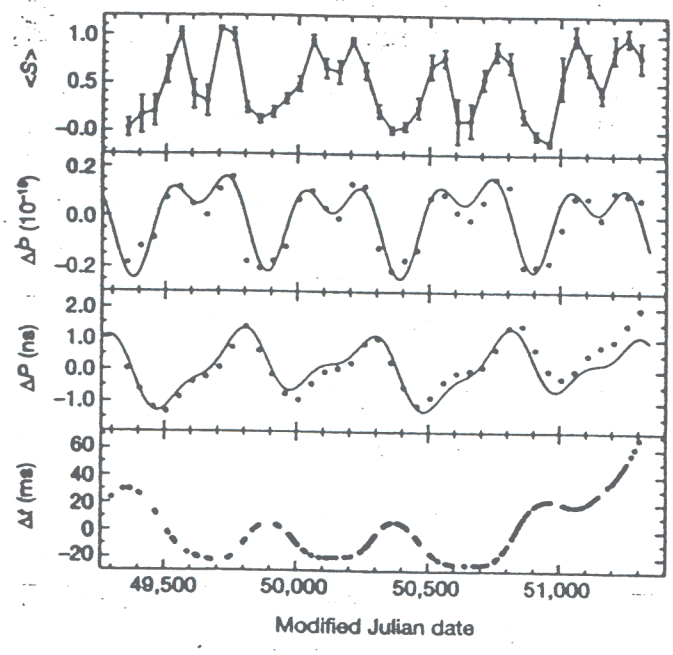

Figure 2 Variations in rotation and pulse shape in PSR B1828–11. The displayed time series are the residuals in arrival time Δt, and period ΔP and derivative $\Delta \dot{P}$, relative to the spin-down model given in Table 1, and the mean pulse shape parameter $\langle S \rangle$ for the most recent 2,000 days, where the observations are most closely spaced. The period residual, ΔP, is the local value of the slope of Δt, and $\Delta \dot{P}$ is the second derivative. The three series ΔP, $\Delta \dot{P}$ and $\langle S \rangle$ were calculated over time intervals of 100 days which overlapped by 50 days. There is, within the uncertainties in $\langle S \rangle$, a clear similarity in form between the variations in $\langle S \rangle$ and in $\Delta \dot{P}$, although this is not obvious from the variations in period or from the observed timing residuals themselves. These periodic patterns continue back through the entire 13-year data set. The solid curves indicate the predictions of a fit of three harmonically-related sinusoids to ΔP; the fundamental period is 1,009 ± 8 days. In addition to modelling ΔP, these fitted parameters, as expected, yield a good representation of $\Delta \dot{P}$.

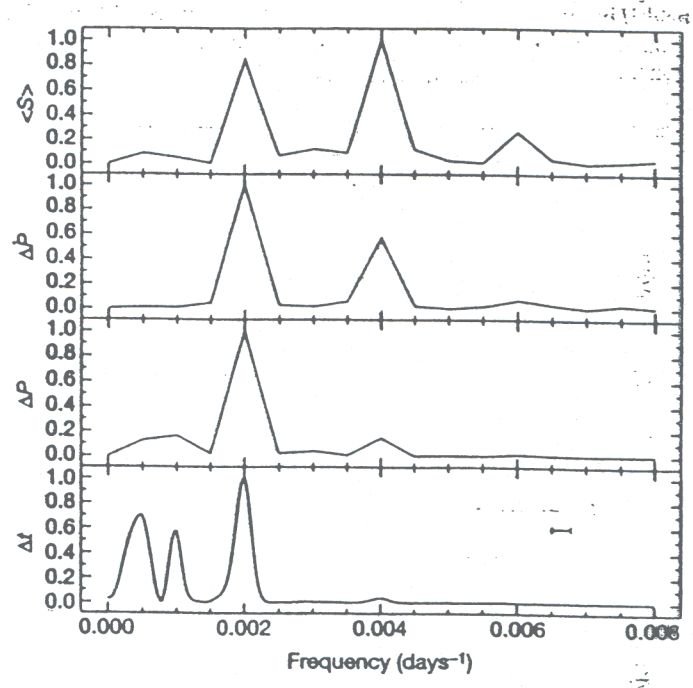

Figure 3 Harmonically related spectral features in the rotation and pulse shape of PSR B1828–11. The panels show the spectral power of the residuals Δt, ΔP, $\Delta \dot{P}$ and the mean pulse shape parameter $\langle S \rangle$. The normalizations are arbitrary. We used a one-dimensional CLEAN algorithm (for example, see ref. 19) for the timing residuals because of the uneven sampling within that data set; the horizontal bar indicates the full width of the smoothing function applied to the timing residual spectrum by this algorithm, and indicates that most of the spectral features are unresolved. The spectra exhibit harmonically related periodicities of approximately 1,000, 500 and 250 days, and confirm that the variations in shape and rotation are related. There is also a strong indication of the presence of a further harmonically related periodicity of approximately 167 days. The relative strengths of the harmonic components in the lower three plots change as expected from successive differentiation of the sinusoidal components of the timing residuals. We note that there is a good chance that the apparent power at around 1/2,000 days in the lowest plot could be due primarily to timing noise in this young pulsar; for this reason we do not include this periodicity in the discussion in the text.

CAN A SUPERFLUID NEUTRON STAR PRECESS FREELY?

- It's trivial.
- It's impossible.
- It's subtle.

IT'S TRIVIAL: EULER

- Conservation of Angular Momentum

$$\frac{d\mathbf{L}}{dt} = \frac{d(\mathbf{I}\cdot\boldsymbol{\Omega})}{dt} = 0$$

- *Rigid rotation* $\equiv$ *zero shear* in corotating frame

$$\frac{d\mathbf{I}}{dt} = \frac{d^{\star}\mathbf{I}}{dt} + \boldsymbol{\Omega}\times\mathbf{I} = \boldsymbol{\Omega}\times\mathbf{I}$$

$$\Rightarrow \mathbf{I}\cdot\left(\frac{d^{\star}\boldsymbol{\Omega}}{dt}\right) + \boldsymbol{\Omega}\times(\mathbf{I}\cdot\boldsymbol{\Omega}) = 0.$$

- Fixed points: $\boldsymbol{\Omega}$ along principal axes of $\mathbf{I}$.

- Linear modes: Two stable, one unstable; energy conservation

- Axisymmetry: Precession frequency

$$\omega_p = \left(\frac{\Delta I}{I}\right)\Omega.$$

ELASTIC SOLID CRUST

• Displacement ξ, strain tensor $u_{ij} = \xi_{(i,k)}$,

$$\text{Shear :} \qquad S_{ij} = u_{ij} - \frac{1}{3}\delta_{ij}\mathrm{Tr}(u).$$

• Stress tensor: Simplest case, isotropic solid

$$\sigma_{ij} = K\delta_{ij}\mathrm{Tr}(u) + 2\mu S_{ij}$$

$K \equiv$ bulk modulus, $\mu \equiv$ shear modulus.

• Euler $\equiv \mu \to \infty$. Zero shear irrespective of applied stress.

• For finite μ,

$$\omega_p = \left(\frac{\Delta I}{I}\right)\Omega \times R$$

$$R \simeq \frac{v_t^2/v_{esc}^2}{1 + v_t^2/v_{esc}^2} \qquad v_t^2 = \frac{\mu}{\rho} \qquad \text{"Rigidity"}$$

(uniform, axisymmetric, self-gravitating).

• A fluid has $\mu = 0 = R \Rightarrow$ cannot precess.

Shear stresses essential for precession.

UNBREAKABLE EGGS

• Frictionless (Poincaré, Kelvin, Lamb, etc.)

$$\omega_p \simeq \left(\frac{\Delta I}{I_{cr}}\right)\Omega$$

$$\omega_w \simeq -\left[1+e\left(1+\frac{2MR^2}{5I_{cr}}\right)\right]\Omega.$$

• Frictional (Bondi & Gold); If there is a frictional force per unit volume $\mathbf{f} = -\beta\Omega\rho\mathbf{u}$ on the fluid, then there are two limits.

Weak Friction $\beta \ll 1$:

$$\delta\omega_p \simeq \left(\frac{2i\beta MR^2}{5I_{cr}}\right)\omega_p \qquad \delta\omega_w \simeq i\beta\Omega\left(1+\frac{2MR^2}{I_{cr}}\right).$$

Strong Friction $\beta \gg 1$:

$$\omega_p \simeq \left(\frac{\Delta I}{I}\right)\Omega\left(1+\frac{2iMR^2}{5\beta I}\right).$$

Other mode rapidly damped.

PINNED SUPERFLUID: SHAHAM (1977) *et sui.*

- Superfluid vorticity organized on quantized vortices, circulation $\kappa = h/2m_n$.

- Vortices move with a velocity $\mathbf{v_L}$ intermediate between local superfluid velocity $\mathbf{v_s}$ and normal fluid velocity $\mathbf{v_n}$.

- *Pinned* vortex lines have $\mathbf{v_L} = \mathbf{v_n}$.

- *Glitch models* suggest vortices are tightly pinned in the neutron star crust $\Rightarrow$ *vorticity* of crustal superfluid fixed in the rotating frame of a perfectly rigid crust $\Rightarrow$

$$\frac{d^\star \mathbf{L_s}}{dt} = 0 = -\mathbf{\Omega}\times\mathbf{L_s} + \mathbf{N}_{s-cr}$$

assuming $\mathbf{L_s} \parallel \omega_\mathbf{s}$. **Euler** changed to

$$\mathbf{I}\cdot\left(\frac{d^\star \mathbf{\Omega}}{dt}\right) + \mathbf{\Omega}\times(\mathbf{I}\cdot\mathbf{\Omega}) = -\mathbf{N}_{s-cr} = -\mathbf{\Omega}\times\mathbf{L_s}$$

$$\Rightarrow \mathbf{I}\cdot\left(\frac{d^\star \mathbf{\Omega}}{dt}\right) + \mathbf{\Omega}\times(\mathbf{L_s} + \mathbf{I}\cdot\mathbf{\Omega}) = 0.$$

- *Fixed Points:* $\mathbf{\Omega} \parallel (\mathbf{L_s} + \mathbf{I}\cdot\mathbf{\Omega})$.

Shaham (cont'd)

• *Linear Modes:* Assuming $\mathbf{L_s}$ along $\mathbf{\Omega}$ in equilibrium,

$$\omega_p = \left(\frac{L_s}{I_{cr}\Omega} + \frac{\Delta I_{cr}}{I_{cr}} \right) \Omega.$$

Generally, far faster than free precession: $\omega_p/\Omega \gg 10^{-7}$. Doesn't matter if the crust is round. (Other mode is $\omega = -\Omega \Rightarrow$ irrelevant.)

• *Coupling to a (Super)Fluid Core:* Assume corotation enforced by a friction-like coupling with timescale $(\Omega\beta)^{-1}$.

Weak Coupling $\beta \ll 1$:

$$\delta\omega_p \simeq \frac{i\beta I_{core}}{I(1+\omega_p/\Omega)}.$$

Rapid oscillations, slowly damped.

Strong Coupling $\beta \gg 1$:

$$\omega_p \simeq \left(\frac{L_s}{I\Omega} + \frac{\Delta I_{cr}}{I} \right) \Omega \left[1 + \frac{iI_{core}}{\beta I} \left(1 + \frac{L_s}{I\Omega} + \frac{\Delta I_{cr}}{I} \right) \right].$$

Rapid oscillations, slowly damped.

GEOMETRIC AND SPINDOWN EFFECTS

(Cordes 1993)

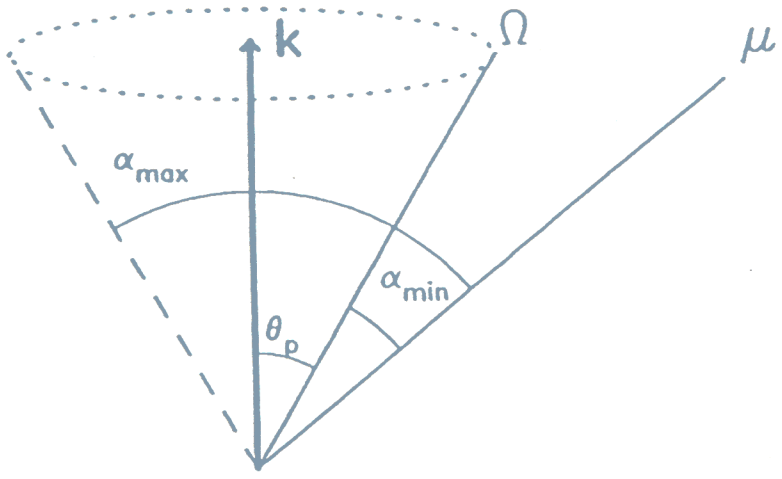

FIGURE III Configuration of axes for free precession in the neutron star frame. The instantaneous angular velocity Ω precesses around the symmetry axis k with frequency ω_p and by an angle θ_p. The magnetic moment μ is fixed with respect to k, while the angle between μ and Ω varies by $\alpha_{max} - \alpha_{min} = 2\theta_p$.

Timing residuals from *geometry* and *spindown*.

AMPLITUDES

$$(\Omega_0 \Delta t)_{\rm geometry} \sim \theta_p$$

$$(\Omega_0 \Delta t)_{\rm spindown} \sim \Gamma_{sd}\theta_p$$

$$\frac{1}{\Omega}\frac{d\Omega}{dt} = -\frac{1}{2\tau}\left[1 - f(\hat{\Omega}\cdot\hat{\rm b})^2\right]$$

$$\Rightarrow \quad \frac{\tau}{t_{sd}} = 1 - f\langle(\hat{\Omega}\cdot\hat{\rm b})^2\rangle \ .$$

$$\Gamma_{sd} = \frac{f\Omega_0}{\omega_p^2 t_{sd}} \simeq 5 f P_p^2({\rm yr}) P_0^{-1} t_{sd,6}^{-1} \ .$$

Spitzer 1958: in *Theoretical Problems of Stellar Magnetism*

We are thus led to the following tentative picture of an idealized magnetic variable star....The angle between the mean dipole field and the angular momentum will be arbitrary. In objects where the angle is appreciable, and where the rate of rotation is moderate, periodic changes of the magnetic field will be observed. Since the axis of rotation usually will not coincide with a principal axis of inertia, hydromagnetic oscillations will be superposed on the variations due to rotation... As the star grows older, the magnetic axis is brought into coincidence with the angular momentum vector...

THE OBLIQUE ROTATOR: Mestel et al.

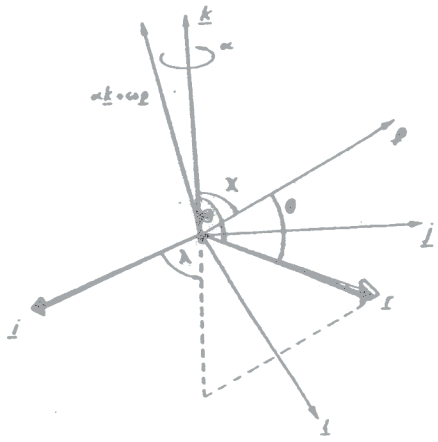

Figure 1. The coordinate system (i, j, k) (spherical coordinates: r, Θ, Λ) is rotating with the star; the system (i, l, p) (spherical coordinates: r, θ, λ) defines the basic magnetic field.

- *Two* "axes of symmetry", $\hat{\Omega}$ and $\hat{\mathrm{b}}$.

$$\rho(\mathbf{r}) = \rho_0(r) + \rho_\Omega(r, \hat{\mathbf{r}}\cdot\hat{\mathbf{\Omega}}) + \rho_B(r, \hat{\mathbf{r}}\cdot\hat{\mathbf{b}})$$

- Moment of inertia tensor

$$\mathbf{I}_{ij} = I_0\delta_{ij} + I_\Omega(\delta_{ij} - 3\hat{\Omega}_i\hat{\Omega}_j) + I_B(\delta_{ij} - 3\hat{\mathbf{b}}_i\hat{\mathbf{b}}_j)$$

$$I_\omega \sim \frac{\Omega^2 R^3}{GM} \qquad I_B \sim \frac{B^2 R^4}{GM^2} \ .$$

- Precession about $\hat{\mathrm{b}}$

$$\omega_p \simeq \frac{3I_B\Omega\hat{\mathbf{b}}(\hat{\mathbf{b}}\cdot\hat{\mathbf{L}})}{I}$$

⋆ DOES IT MATTER? ⋆

NO

- VERY slow

$$\omega_p = \frac{3I_B\Omega\cos\chi}{I} \simeq 2\times 10^{-12}\Omega\beta\cos\chi B_{24}^2 R_6^4 M_{1.4}^{-2} I_{45}^{-1}$$

$\Rightarrow$ precession period $\sim 10^{12}$ rotation periods i.e. perhaps $10^4 - 10^5$ years.

- $\hat{\mathbf{b}}$ rotates uniformly, so there is no geometric variation in arrival time or beam inclination.

- $\hat{\mathbf{b}}\cdot\hat{\mathbf{\Omega}}$ does not vary, so there are no torque-induced phase residuals.

MAYBE: TYPE II SUPERCONDUCTIVITY

Jones '75, Easson & Pethick 1977, Cutler 2002

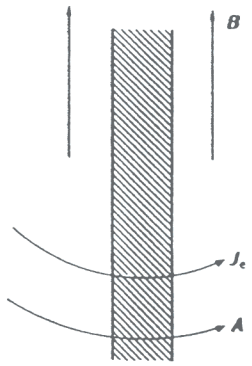

Figure 6.24 Magnetic field B, supercurrent J_e and vector potential A in a vortex line in a superconductor.

- Quantized flux lines $\phi_0 = hc/2e$, confined within a penetration depth $\lambda_p \simeq (m_p c^2/4\pi n_p e^2)^{1/2} \simeq 10^{-11}$ cm from axis; $\lambda_p > \xi_p\sqrt{2}$ coherence length.

- Larger than Maxwell stress: $B^2 \to BH_{c1}$ where the first critical field strength $H_{c1} \simeq 10^{15}$ Gauss for neutron stars.

- Distortion enhanced, precession faster:

$$\omega_p = \frac{3I_B\Omega\cos\chi}{I} \simeq 2\times10^{-9}\Omega\beta\cos\chi(BH)_{27}R_6^4M_{1.4}^{-2}I_{45}^{-1}$$

- *BUT*:
  - ⋆ Fluid precesses about $\hat{\mathbf{b}}$.
  - ⋆ $\hat{\mathbf{b}}\cdot\hat{\mathbf{\Omega}}$ remains unchagned.

BREAKING THE SYMMETRY: A CRUST

- Add moment of inertia of the crust, C_{ij}.
- *Steady state* only if $\mathbf{\Omega}$ is along a principal axis of

$$\Delta_{ij} = C_{ij} + I_B \left(\delta_{ij} - 3 I_B \hat{\mathbf{b}}_i \hat{\mathbf{b}}_j \right)$$

  - ⋆ When $C_{ij} = 0$, requires $\hat{\mathbf{\Omega}} \cdot \hat{\mathbf{b}} = 0$ or 1.
  - ⋆ When $I_B = 0$, requires $\hat{\mathbf{\Omega}}$ along a PA of C_{ij}.

- Example: Axisymmetric crust $C_{ij} = C \left(\hat{\mathbf{k}}_i \hat{\mathbf{k}}_j - \delta_{ij} \right)$

If $\cos\theta = \hat{\mathbf{b}} \cdot \hat{\mathbf{k}}$ and $\cos\chi = \hat{\mathbf{b}} \cdot \hat{\mathbf{\Omega}}$ require

$$\sin 2(\chi - \theta) = \frac{I_B \sin 2\chi}{C}$$

for steady state.

⋆ STEADY STATE MAY BE IMPOSSIBLE ⋆

Aside: Minimum Energy State(s)

- *Define* χ at instant when $\hat{\mathbf{b}}$, $\hat{\mathbf{k}}$ and $\hat{\boldsymbol{\Omega}}$ are *coplanar.*

- *Energy Extrema* when

$$\sin 2(\chi - \theta) = 0$$

$$\sin 2(\chi - \theta) = \frac{I_B \sin 2\chi}{C}$$

Requires $\theta = \chi$ *and* $\chi = 0$ or $\pi/2$.

- *Local* ($\theta = \chi$) versus *Global* ($\chi = 0$ or $\pi/2$) energy minima.

Precession is *REQUIRED* for large $|I_B/C|$.

Local energy minima precess.

TRIAXIAL PRECESSION

- Axisymmetric crust + Axisymmetric magnetic distortion $\Rightarrow$ Triaxial ΔI_{ij}.
- Most interesting case: $I_B \gg C$.

$\star\star$ NOT JUST TRIAXIAL PRECESSION $\star\star$

- *Fluid* precesses at *large* amplitude χ $\Rightarrow$
  - $\star$ Vortex unpinning easy.
  - $\star$ Comparable harmonics easy.
- *Magnetic axis* precesses at *small* amplitude $\sim C/I_B$ $\Rightarrow$ arrival times, $\hat{\mathbf{b}}$.

Timing Residuals ($I_B > 0$)

$$\Omega_0 \Delta t_{osc} = (\text{geometric}) + (\text{spindown})$$

$$\frac{\text{geometric}}{C/I_B} = \left(\frac{\sin^2\theta \sin 2\omega_p t}{4\cos\chi} - \frac{\sin 2\theta \sin \omega_p t}{2\sin\chi} \right)$$

$$\frac{\text{spindown}}{C/I_B} = \Gamma_{sd} \left(\frac{\sin^2\theta \cos 2\omega_p t}{16} + \frac{\cos\chi \sin 2\theta \cos\omega_p t}{2\sin\chi} \right) .$$

APPLICATION TO PSR 1828-11

- Precession period

$$P_p \simeq \frac{500 \text{ days}}{\beta \cos\chi (B H_{27}/5)}$$

- $I_B > 0$ superior to $I_B < 0 \Rightarrow$ *PROLATE*

- Unexceptional χ (e.g. 60 degrees) allowed (if not favored).

- Amplitude requires $fC/I_B \sim 0.01 - 0.001$. Can be consistent with reasonable pulse shape changes, depending on beam shape.

Implications of PROLATE:

⋆ Toroidal, not Type II?

⋆ Outward transport of flux tubes
(Ruderman, Zhu & Chen 1998)

EVIDENCE FOR TYPE II SUPERCONDUCTIVITY?

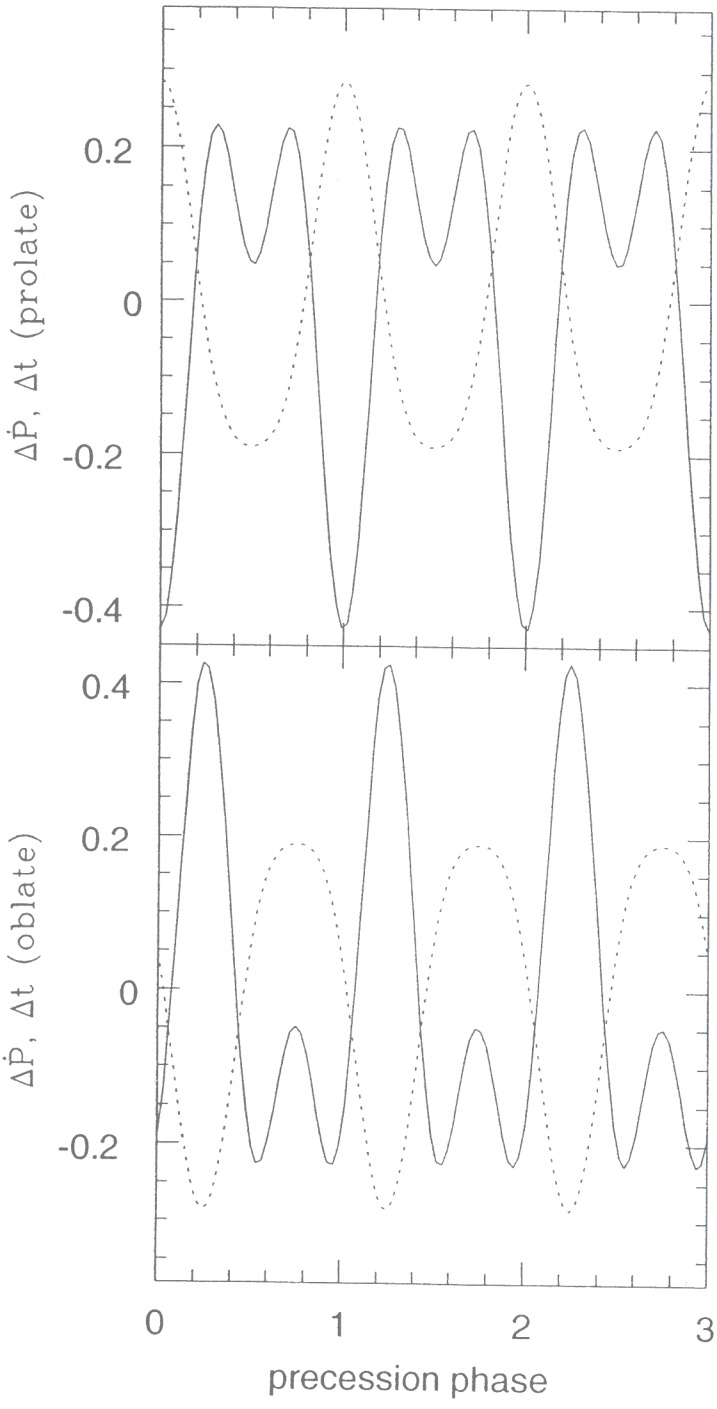
0.2
0
-0.2
-0.4
ΔṖ, Δt (prolate)
0.4
0.2
0
-0.2
ΔṖ, Δt (oblate)
0
1
2
3
precession phase

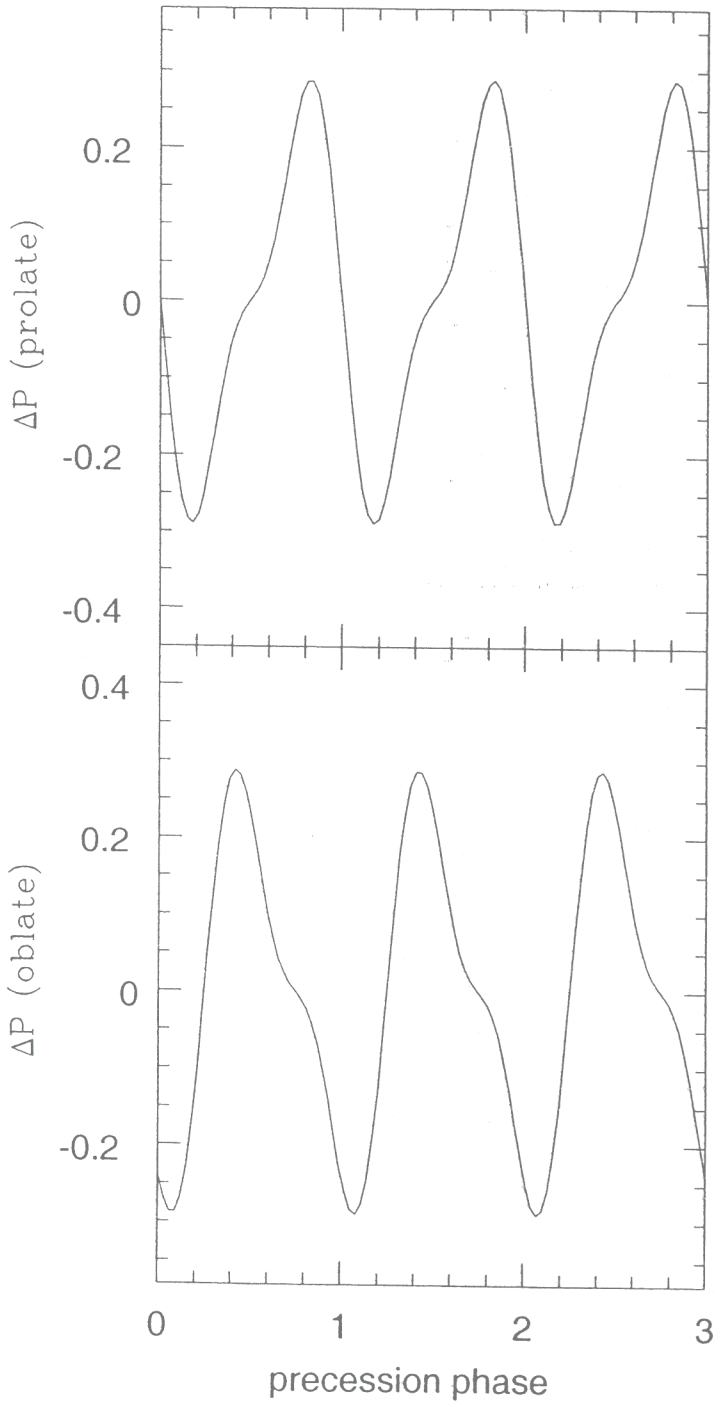
0.2
0
-0.2
-0.4
ΔP (prolate)
0.4
0.2
0
-0.2
ΔP (oblate)
0
1
2
3
precession phase

WEAK COUPLING TO CRUST WITH PINNING?

- Suppose: (1) Pinning in crust. (2) Distorted core
- Assume: Crust-core coupling weak
  (timescale $\sim \gamma^{-1}$ rotation; $\gamma \ll 1$)

Result: *Slowly damped precession* $\sigma \simeq \epsilon\hat{\Omega}_3(1 + i\gamma)$

- Angular velocity $\rightarrow \parallel$ or $\perp$ core symmetry axis
- Nonlinear $\Rightarrow$ precession frequency varies.
- Crustal $\hat{\mu}$ oscillates at twice the precession frequency, with amplitude $\sim \gamma\hat{\Omega}_3(1 - \hat{\Omega}_3^2) = \gamma \cos\chi \sin^2\chi$.

Application to PSR 1828-11

- *Damping* slower than *spindown* $\Rightarrow$ $\gamma \lesssim 10^{-5}$ $\Rightarrow$ amplitude too small: $\Delta\dot{P} \sim 10^{-18}$, not 10^{-16}.
- $\gamma \sim 10^{-3}$ $\Rightarrow$ *amplitude still too small* ($\rightarrow \parallel$ or $\perp$)
- *Unless* symmetry axis of core *time variable*, not simply related to $\hat{\mu}$ for crust.

GOOD AND BAD POINTS

- Magnetic fields are central to pulsar phenomenon, why not to precession?

- Type II superconductivity possible in core; toroidal fields $\sim 10^{15\frac{1}{2}}$G possible alternative.

- Precession frequency (if Type II) consistent with estimated magnetic stresses

- Crust-core coupling strong in simplest solutions, amplitude determined by C/I_B. Obliquity arbitrary.

- C and I_B connected ? (future work)

- Crust-core coupling weak possible, but only if precession is re-excited episodically.

- If this is true, why don't *all* pulsars precess?

CHALLENGES

- Why isn't precession observed in all radiopulsars?
  - ⋆ Precessors vs. glitchers.
  - ⋆ Timing noise and precession?
  - ⋆ Larger amplitudes ⇒ beams not in our line of sight often enough?
- Angular dependence of spindown torque? A probe?
- Multicomponent models, relaxation
  - ⋆ Dissipation (SWC); but might be slow.
  - ⋆ MHD, elastic deformations, distortions.
  - ⋆ Crust/core MHD oscillations via shearing fields?
- Is precession precession?
  - ⋆ Slow MHD branch of inertial modes (Hide 1974); but absent with shear stress.
  - ⋆ Vortex lattice oscillations (Tkachenko); but lattice destroyed by pinning; Tkachenko modes deep inside do not affect outer crust.
  - ⋆ Must the slow modes be associated with the star? (Example: LT frequency is $\sim 10^{-7}\Omega$ at $r/R \sim 100$

– inside light cylinder, but probably higher than altitude of radio emission.)

• Young, fast rotators with/without strong magnetic fields? Will we miss them because beams precess out of line of sight?

• Gravitational radiation.

• Can Shaham mode be observed in radiopulsars?

OUTLOOK

Two viable models (maybe three)

⋆ Axisymmetric, $\theta \simeq 3$ degrees, $\chi \simeq 89$ degrees (Link & Epstein 2001).

⋆ Magnetic, triaxial, χ not highly constrained, amplitude set by C/I_B, prolate.

Both rely on spindown for allowing large enough residuals, small enough wobble.